Biochimica et Biophysica Acta 1808 (2011) 382–393

Contents lists available at ScienceDirect

Biochimica et Biophysica Acta

journal homepage: www.elsevier.com/locate/bbamem

Different membrane behaviour and cellular uptake of three basic arginine-rich peptides

Astrid Walrant [a], Isabelle Correia [a], Chen-Yu Jiao [a], Olivier Lequin [a], Eric H. Bent [a], Nicole Goasdoué [a], Claire Lacombe [a,b], Gérard Chassaing [a], Sandrine Sagan [a], Isabel D. Alves [a,*]

[a] UMR 7203 UPMC CNRS, Laboratoire des BioMolécules, Paris F-75005, France
[b] UFR Sciences et Technologie, UPEC, Créteil, France

ARTICLE INFO

Article history:
Received 5 July 2010
Received in revised form 15 September 2010
Accepted 16 September 2010
Available online 13 October 2010

Keywords:
Cell penetrating peptide
Polyarginine
Cellular uptake
Peptide lipid interactions
Calorimetry
NMR

ABSTRACT

Cell penetrating peptides (CPPs) are peptides displaying the ability to cross cell membranes and transport cargo molecules inside cells. Several uptake mechanisms (endocytic or direct translocation through the membrane) are being considered, but the interaction between the CPP and the cell membrane is certainly a preliminary key point to the entry of the peptide into the cell. In this study, we used three basic peptides: RL9 (RRLLRRLRR-NH_2), RW9 (RRWWRRWRR-NH_2) and R9 (RRRRRRRRR-NH_2). While RW9 and R9 were internalised into wild type Chinese Hamster Ovary cells (CHO) and glycosaminoglycan-deficient CHO cells, at 4 °C and 37 °C, RL9 was not internalised into CHO cells. To better understand the differences between RW9, R9 and RL9 in terms of uptake, we studied the interaction of these peptides with model lipid membranes. The effect of the three peptides on the thermotropic phase behaviour of a zwitterionic lipid (DMPC) and an anionic lipid (DMPG) was investigated with differential scanning calorimetry (DSC). The presence of negative charges on the lipid headgroups appeared to be essential to trigger the peptide/lipid interaction. RW9 and R9 disturbed the main phase transition of DMPG, whereas RL9 did not induce significant effects. Isothermal titration calorimetry (ITC) allowed us to study the binding of these peptides to large unilamellar vesicles (LUVs). RW9 and R9 proved to have about ten fold more affinity for DSPG LUVs than RL9. With circular dichroism (CD) and NMR spectroscopy, the secondary structure of RL9, RW9 and R9 in aqueous buffer or lipid/detergent conditions was investigated. Additionally, we tested the antimicrobial activity of these peptides against *Escherichia coli* and *Staphylococcus aureus*, as CPPs and antimicrobial peptides are known to share several common characteristics. Only RW9 was found to be mildly bacteriostatic against *E. coli*. These studies helped us to get a better understanding as to why R9 and RW9 are able to cross the cell membrane while RL9 remains bound to the surface without entering the cell.

1. Introduction

For the past 15 years, cell penetrating peptides (CPPs) have attracted much attention. Indeed, their unique ability to cross the plasma membrane designates them as potentially very powerful vectors to transport molecules that would otherwise never penetrate into cells such as heavily negatively charged polynucleic acids or some small molecules with therapeutic interest [1]. Since the discovery of penetratin, the third helix of the Antennapedia homeodomain [2,3], and of the HIV Tat peptide [4,5] in the 1990s, there has been extensive work to develop new synthetic and powerful CPPs such as polyarginines [6,7]. Many of these peptides share common features, namely a high density in basic residues and an amphipathic secondary structure in membrane environments. Together with the design of new peptides, there has been massive investigation on the internalisation mechanisms of CPPs. Indeed, a good understanding of the internalisation routes is essential for the development of efficient vectors. Cellular uptake mechanism is highly controversial, and both

Abbreviations: APA, Amino pentanoic acid; CD, Circular dichroism; CHO, Chinese hamster ovary; CPP, Cell-penetrating peptide; CS, Chondroitin sulfate; CSD, Chemical shift deviation; D8PG, Dioctanoyl phosphatidylglycerol; DiPoPE, Dipalmitoleoyl phosphatidylethanolamine; DLS, Dynamic light scattering; DMPC, Dimyristoyl phosphatidylcholine; DMPG, Dimyristoyl phosphatidylglycerol; DPC, Dodecyl phosphocholine; DSC, Differential scanning calorimetry; DSPG, Distearoyl phosphatidylglycerol; HS, Heparan sulfate; HSQC, Heteronuclear single quantum correlation; ITC, Isothermal titration calorimetry; LDH, Lactate dehydrogenase; LUV, Large unilamellar vesicle; MIC, Minimal inhibitory concentration; MLV, Multi lamellar vesicle; NOE, Nuclear Overhauser effect; NOESY, NOE spectroscopy; PA, Phosphatidic acid; PC, Phosphatidylcholine; PE, Phosphatidylethanolamine; PG, Phosphatidylglycerol; PI, Phosphatidylinositol; PS, Phosphatidylserine; SDS, Sodium dodecyl sulfate; TOCSY, Total correlation spectroscopy

* Corresponding author. UMR 7203 UPMC CNRS, Laboratoire des BioMolécules, case courrier 182, 4, Place Jussieu, 75005 Paris, France. Fax: +33 1 44 27 71 50.
E-mail address: isabel.alves@upmc.fr (I.D. Alves).

0005-2736/$ – see front matter © 2010 Elsevier B.V. All rights reserved.
doi:10.1016/j.bbamem.2010.09.009

endocytosis and direct translocation through the membrane are being discussed. Independently from their internalisation mechanisms, the interaction between the CPP and the cell membrane should be a preliminary key point to be taken into account. In this perspective, the study of the interaction of peptides with model lipid membranes can provide precious information about the phenomena that may occur at the cell surface. Cellular membranes can be simulated by very simple objects such as detergent micelles or lipid monolayers, or by more complex models such as multi-lamellar vesicles (MLVs) or large unilamellar vesicles (LUVs). The diversity of membrane models gives access to a very large array of biophysical techniques to study peptide/lipid interactions.

In this study, we chose to investigate the membrane behaviour of three arginine-rich peptides: the well known nona-arginine R9 peptide (RRRRRRRRR-NH_2) and two amphipathic peptides with a similar charge distribution, RW9 (RRWWRRWRR-NH_2) and RL9 (RRLLRRLRR-NH_2). The RW9 and RL9 peptides derive from the 16-mer sequences RW16 (RRWRRWWRRWWRRWRR-NH_2) and RL16 (RRLRRLLRRLLRRLRR-NH_2) respectively, which were designed from penetratin [8]. The three studied peptides RW9, RL9 and R9 share a common high density of arginine residues, which confers nine positive charges to R9 and six positive charges to RW9 and RL9.

It is well established that polyarginines such as R9 are very potent CPPs [6]. Different studies also showed that RW9 is efficiently internalised into cells [9,10]. Surprisingly, we found, using mass spectrometry quantification methods [11], that RL9 is very poorly internalised by cells. Therefore, the behaviour of these three peptides was studied in the presence of membrane models (MLVs and LUVs) in an attempt to correlate their different cellular uptake with a distinct behaviour at the level of lipid/peptide interactions. Herein, the thermodynamics of peptide interaction with lipid model systems was investigated, both in terms of affinity and peptide induced perturbation of the lipid phase transition using isothermal titration calorimetry (ITC) and differential scanning calorimetry (DSC), respectively. Additionally, the peptide structural changes accompanying lipid interaction were monitored by circular dichroism (CD) and NMR spectroscopy. Finally, since CPPs and antimicrobial peptides share common features [12], the antimicrobial activities of these peptides were investigated against *Escherichia coli* and *Staphylococcus aureus*.

2. Materials and methods

2.1. Materials

DMPC, DMPG and DSPG were obtained as a powder from Genzyme (Switzerland). DiPoPE and D8PG were purchased from Avanti Polar Lipids (Alabaster, AL). DPC-d_{38} was purchased from Eurisotop (Saint-Aubin, France). Biot(O_2)-Apa-RW9, Biot(O_2)-Apa-R9, Biot-$(Gly)_4$-RL9 and Biot-([2,2-D_2]-$Gly)_4$-RL9 were obtained from PolyPeptide Laboratories (Strasbourg, France). Biot(O_2)-Apa-RL9, Biot(O_2)-$(Gly)_4$-RW9 and Biot(O_2-([2,2-D_2]-$Gly)_4$-RW9 were synthesised using the Boc-solid phase strategy. Peptides used in most experiments have the Biot(O_2)-Apa N-terminal extension, except in quantification studies where the peptides have the Biot(O_2)-$(Gly)_4$ N-terminal extension (Section 2.4).

2.2. Cell culture

Wild type Chinese Hamster Ovary CHO-K1 cells and xylose transferase-deficient CHO-pgsA745 cells were cultured in Dulbecco's modified Eagle's medium (DMEM) supplemented with 10% foetal calf serum (FCS), penicillin (100,000 IU/L), streptomycin (100,000 IU/L), and amphotericin B (1 mg/L) in a humidified atmosphere containing 5% CO_2 at 37 °C.

2.3. Cytotoxicity and membrane integrity

Cytotoxicity was measured using the Dojindo Cell-Counting Kit 8 based on the reduction of a reagent into a coloured product by viable cell dehydrogenases. CHO-K1 cells were seeded in a 96-well plate 1 day before treatment (4000 cells per well). Cells were treated with 0.1 μM, 1 μM, 5 μM and 20 μM peptide for 1 h, 3 h, 6 h, 16 h and 24 h. Untreated cells were defined as zero (negative control), and 1% SDS as maximum cytotoxicity (positive control).

Membrane perturbation was measured using the Promega CytoTox-ONE kit based on the quantification of lactate dehydrogenase (LDH) leakage. CHO-K1 cells were seeded in a 96-well plate (10,000 cells per well) 1 day before treatment. The same conditions as for cytotoxicity assays were used. Maximum LDH release was induced by treatment with 0.2% Triton X-100.

2.4. Measure of cellular uptake and quantification of membrane-bound peptide

Cellular uptake was quantified using the method described by Burlina et al [13]. In this protocol, the studied peptide bears a tag composed of four glycine residues together with a biotin moiety for purification purposes. After 1 h incubation of 7.5 μM peptide and washing, a protease is added (0.05% Pronase in Tris–HCl buffer, 100 mM pH 7.5) in order to detach the cells and to degrade all the non-internalised or membrane-bound peptide. This avoids overestimating the quantity of internalised peptide due to the presence of peptides attached to the outer leaflet of the membrane. The cells are then lysed (0.3% Triton) and boiled and the cell lysate is then incubated with streptavidin-coated magnetic beads to extract the peptide from the lysate. For membrane-bound peptide quantification, the same experimental conditions were used except that no protease was added and the cells were directly lysed. The peptides are eluted from the streptavidin-coated magnetic beads with HCCA matrix and spotted on the MALDI plate. Mass spectrometry is not a quantitative method *per se*, therefore an internal standard is added to the lysis solution. This standard peptide has the same sequence as the one to quantify except that it bears a tag composed of four deuterated glycine residues instead of four glycine residues. This allows the quantification of internalised and membrane-bound peptide. The samples were analysed by MALDI-TOF MS (positive ion reflector mode) on a Voyager DEPRO mass spectrometer (Applied Biosystems).

2.5. Antimicrobial activity

Gram-positive eubacteria (*S. aureus* RN4220) and Gram-negative eubacteria (*E. coli* ML35p) were grown in Luria–Bertani (LB) broth at 37 °C. The minimal inhibitory concentrations (MICs) of peptides were determined in 96-well microtitration plates by growing the bacteria in the presence of 2-fold serial dilutions of peptide ranging from 0.2 to 100 μM. Aliquots (10 μL) of each serial dilution were incubated for 16 h at 37 °C with 90 μL of a suspension of a midlogarithmic phase culture of bacteria at a starting absorbance $A_{630} = 0.05$ in Poor Broth nutrient medium (1% Casein peptone and 1% NaCl, w/v). Growth inhibition was assayed by measuring the absorbance at 630 nm. The MIC was defined as the lowest concentration of peptide that inhibited the growth of 99% or more of the bacteria. 0% inhibition corresponded to untreated bacteria (negative control), 100% inhibition corresponded to bacteria treated with 0.2% formaldehyde (positive control).

If a MIC could be determined, then 2 μL of the bacterial suspension that was incubated with a concentration of peptide corresponding to the MIC and the concentration just above the MIC were taken, plated out on solid culture medium containing 1% noble agar and incubated overnight at 37 °C. If the bacteria were able to re-grow, the peptide was described as bacteriostatic, otherwise the peptide was described as bacteriolytic.

2.6. Preparation of MLVs and LUVs

Lipid films were made by dissolving the appropriate amount of lipid into chloroform or a mixture of chloroform and methanol (2/1 vol/vol). The solvent was then evaporated under nitrogen to deposit the lipid as a film on the wall of a test tube. Final traces of solvent were removed in a vacuum chamber attached to a liquid nitrogen trap during 3–4 h. Films were then hydrated with 10 mM Tris, 0.1 M NaCl, 2 mM EDTA, pH 7.6 for DSC and ITC experiments. For CD experiments, lipid films were hydrated with 10 mM sodium phosphate buffer pH 7.6. The films were then vortexed extensively at a temperature superior to the phase transition temperature of the lipid to obtain MLVs. To form LUVs, the MLVs were subjected to five freeze/thawing cycles. For low concentration of lipids (~1 mg/mL), the homogeneous lipid suspension was passed 19 times trough a mini-extruder (Avanti Alabaster, AL) equipped with two stacked 100 nm polycarbonate membranes at a temperature above the phase transition temperature of the lipid. For higher concentrations of lipids (~10 mg/mL), the homogeneous lipid suspension was passed 10 times trough a nitrogen pressure driven extruder (LIPEX, Northern Lipids Inc., BC) equipped with a 100 nm polycarbonate membrane at a temperature above the phase transition temperature of the lipid.

2.7. Differential scanning calorimetry (DSC)

DSC experiments were performed on a high-sensitivity calorimeter (TA Instruments). A scan rate of 1 °C/min was used and there was a delay of 10 min between sequential scans in a series to allow thermal equilibration. Data analysis was performed by the fitting program NanoAnalyze provided by TA Instruments. The lipid concentration was 1 mg/mL, except for experiments with DiPoPE where a concentration of 10 mg/mL of lipid was used, due to the weaker DSC signal displayed by this lipid. Biot(O_2)-Apa-RL9, Biot(O_2)-Apa-RW9 or Biot(O_2)-Apa-R9 were gradually added to the lipid MLVs to obtain peptide/lipid molar ratios of 1/100, 1/50, 1/25 and 1/10, except for experiments with DiPoPE where a peptide/lipid ratio of 1/25 was used. A minimum of at least three to four heating and cooling scans were performed for each analysis.

2.8. Isothermal titration calorimetry (ITC)

ITC experiments were performed on a TA Instrument nano ITC calorimeter. To avoid air bubbles, peptide and LUVs solutions were degassed under vacuum before use. Titrations were performed by injecting aliquots of LUVs (lipid concentration varying between 12.48 mM and 6.24 mM) into the calorimeter cell containing the peptide solution (peptide concentration 0.1 mM), with 5 min waiting between injections. The experiments were performed at 25 °C. Data analysis was performed using the program NanoAnalyze provided by TA Instruments.

2.9. Turbidity measurements

Turbidity changes in LUVs and MLVs suspensions following peptide addition (at P/L ratios of 1/100, 1/50, 1/25 and 1/10) were monitored by absorbance measurement at 436 nm. Peptide was gradually added to 500 µL of lipid LUVs/MLVs suspensions (at 1 mg/mL of lipid) in 10 mM phosphate buffer. Absorbance was measured on a UVICON 930 spectrophotometer at room temperature.

2.10. Circular dichroism experiments

The CD spectra of the peptides were recorded on a Jobin Yvon CD6 dichrograph linked to a PC microprocessor. The spectra were recorded at 25 °C in a quartz optical cell with a 1 mm path length from 185 to 260 nm with a 0.5-nm step. Four scans were accumulated and averaged after buffer (or LUV) spectra subtraction and baseline correction. The spectra were acquired for peptide concentrations varying from 28 µM to 127 µM (corresponding to peptide to lipid ratios of 1/50 to 1/10) in phosphate buffer or in the presence of lipid LUVs (1 mg/mL). CD measurements were reported as $\Delta\varepsilon$ (M^{-1} cm^{-1}).

2.11. NMR spectroscopy

The peptide samples were prepared at 1 mM concentration in 550 µL of H_2O/D_2O (90:10 v/v) containing 50 mM sodium phosphate at pH ~6. Sodium 2,2-dimethyl-2-silapentane-d_6-5-sulfonate (DSS, Isotec) was added (0.1 mM) for direct ^{1}H and indirect ^{13}C chemical shift calibration. Micellar samples additionally contained 60 mM DPC-d_{38} or 60 mM SDS, corresponding to a ratio of ~1 peptide per micelle. Spectra of micellar samples were indirectly calibrated to the aqueous samples due to interaction of DSS with the micelles.

NMR spectra were recorded on a Bruker Avance III spectrometer, operating at a ^{1}H frequency of 500.11 MHz, and equipped with a triple-resonance Z-gradient TCI cryoprobe. One-dimensional spectra were recorded between 10 and 40 °C and 2D experiments were recorded at 20 or 35 °C. The following 2D experiments were recorded: TOCSY (DIPSI-2 mixing sequence [14] with durations of 22 and 60 ms), NOESY (mixing times of 50 and 125 ms) and natural abundance ^{1}H–^{13}C HSQC. The solvent signal was suppressed using a WATERGATE sequence and water flip back pulses in homonuclear experiments recorded on aqueous or micellar DPC samples [15,16]. For homonuclear experiments recorded on non-deuterated SDS samples, a double pulsed field gradient spin echo [17] was employed with selective pulses centered on the amide/aromatic region (90° G4 shaped pulse of 4 ms and 180° RE-BURP shaped pulse of 3 ms). Gradient pulses were used for coherence selection in HSQC experiments. Vicinal $^{3}J_{HN\text{-}H\alpha}$ coupling constants were measured on 1D spectra for peptides in aqueous solutions. Coupling constants could not be measured in micellar environments due to resonance broadening.

NMR data were processed and analysed with Bruker TOPSPIN 2.0 program. Time-domain data were typically apodised with shifted sine-bell or squared sine-bell window functions, and zero-filled twice prior to Fourier transformation. Indirect dimensions were extended by linear prediction. Baseline distortions were corrected with a fifth-order polynomial function.

2.12. NMR structure calculations

Interproton distance restraints were estimated from NOESY cross-peak volumes. The calibration was based on cross-peaks involving aromatic Trp $HN^{\varepsilon 1}$-$H^{\zeta 2}$ protons (2.9 Å). For each peptide, a set of 50 structures was calculated by torsion angle dynamics in DYANA using standard parameters [18]. The best 25 structures exhibiting the lowest target function were then minimised using XPLOR-NIH program [19]. CHARMM22 forcefield was used and non-bond energy terms consisted of a Lennard–Jones potential and an electrostatic term with a distance-dependent dielectric $\varepsilon = 4r$ and a cutoff of 8 Å. Structures were analysed with InsightII, MOLMOL and PROCHECK-NMR programs.

3. Results and discussion

3.1. Cell membrane integrity and cytotoxicity

A prerequisite for a peptide to be a potential CPP is that it is not toxic towards mammalian cells. Cytotoxicity was assayed on CHO cells by measuring the number of viable cells and cell membrane integrity was assayed by quantifying LDH leakage after incubation with peptide. Concentrations from 0.1 to 20 µM of peptide (corresponding to the range of concentrations employed for internalisation studies) were used. Incubation times ranged from 1 to 24 h. None of the three

peptides showed any cytotoxicity or significant membrane perturbation even at the highest peptide concentration (20 μM) and longest incubation time (24 h) tested (data not shown).

3.2. Antimicrobial activity

Since several CPPs show antimicrobial activity [20] and share some common features with antimicrobial peptides [12], the antimicrobial activities of RL9, RW9 and R9 were assayed against two bacterial strains: *E. coli* (Gram-negative) and *S. aureus* (Gram-positive). RL9 and R9 showed no activity against either strain, even at the highest tested concentration (100 μM). On the other hand, RW9 proved to have mild antimicrobial activity (Table 1). When incubated with 100 μM of RW9 for 24 h, 99% of *S. aureus* growth was inhibited. On *E. coli*, at a concentration of 25 μM RW9, 99% of growth was inhibited after 24 h incubation. Furthermore, the bacteria were able to re-grow after being incubated with RW9 at 25 μM and 50 μM, showing that RW9 is bacteriostatic but not bacteriolytic against *E. coli*. We did not test whether RW9 was bacteriolytic or bacteriostatic against *S. aureus* as the MIC (100 μM) is not biologically relevant.

Membranes of bacteria and eukaryotic cells differ in many aspects, amongst which their lipid composition. Eukaryotic cell membranes contain essentially zwitterionic lipids such as phosphatidylcholine lipids (PC) whereas bacterial membranes are rich in negatively charged lipids such as phosphatidylglycerol lipids (PG). As will be shown in Sections 3.4 and 3.5, RL9, RW9 and R9 mainly interact with anionic lipids and for that reason these peptides could potentially have had antimicrobial activity. Indeed, most antimicrobial peptides act against bacteria by disrupting (lysis, pore formation...) the negatively charged bacterial membrane [21,22].

3.3. Quantification of internalised and membrane-bound peptide

The quantification of internalised and membrane-bound RL9 and RW9 was performed using two cell lines: wild type CHO-K1 cells and heparan sulphate (HS) and chondroitin sulphate (CS) proteoglycan-deficient CHO-pgsA 745 cells. This allowed us to study the role of these proteoglycans in the internalisation and membrane binding processes. Furthermore, the experiments were performed at two temperatures: 37 °C and 4 °C. At 4 °C peptides can only enter the cell through direct translocation, since endocytosis, an energy-dependent process, is inhibited this temperature. The cellular uptake and membrane-bound peptide quantification experiments for R9 and RW9 had already been performed by the same method [10]. They were not repeated for R9, but they were in the case of RW9 as the N-terminal tag was different.

3.3.1. Quantification of internalisation

Internalisation studies have already showed that RW9 is a very efficient CPP [9,10]. Our results, which are displayed in Fig. 1, confirmed this observation. At 37 °C, RW9 was internalised to an intracellular concentration of 10 μM in CHO-K1 cells, which makes it, together with R9, one of the most efficient known CPPs. In CHO-pgsA 745 cells, RW9 was still internalised, but to a lesser extent than in CHO-K1 cells (around 4 μM) suggesting that cell surface HS and CS play a role in the internalisation. At 4 °C, RW9 was still able to enter both cell types, showing that RW9 has the ability to translocate directly through the lipid bilayer. Direct translocation of an arginine-tryptophan peptide, R7W, had already been reported, together with penetratin and R7 [23]. On the other hand, RL9 was extremely poorly internalised (approximately 0.5 μM) in CHO-K1 cells as well as CHO-pgsA 745 cells, and was hardly detectable inside the cells. As a comparison, R9 is as successfully internalised by CHO-K1 and CHO-745 cells as RW9 at 37 °C. However, R9 is internalised to higher amounts at 4 °C than RW9, showing that R9 translocates more efficiently through the lipid bilayer. So oligoarginine peptides enter cells both by direct translocation and endocytosis, in agreement with previous studies from other laboratories [23–26].

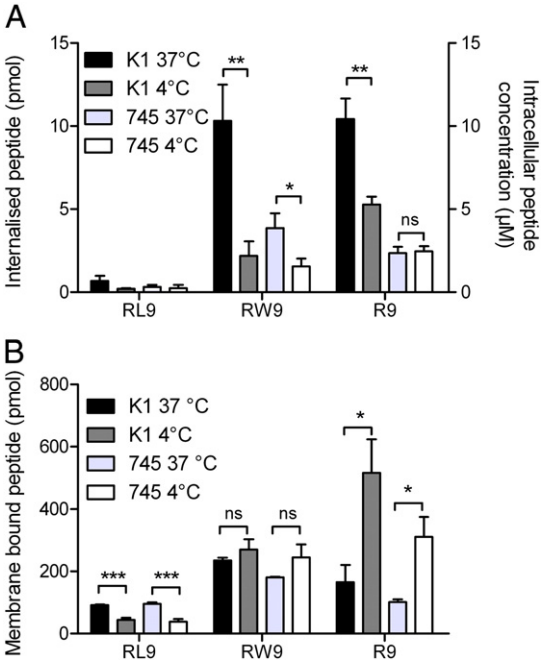

Fig. 1. Quantification of internalised and membrane-bound peptide in CHO-K1 and CHO-pgsA 745 cells at 37 °C and 4 °C. (A) Internalised peptide (pmol) or intracellular concentrations (μM) of RL9 (left), RW9 (middle) and R9 (right) into CHO-K1 at 37 °C (black) and 4 °C (dark grey) and into CHO-pgsA 745 at 37 °C (light grey) and at 4 °C (white) ($n \geq 8$). (B) Membrane bound peptide (pmol) of RL9 (left), RW9 (middle) and R9 (right) on CHO-K1 at 37 °C (black) and 4 °C (dark grey) and on CHO-pgsA 745 at 37 °C (light grey) and at 4 °C (white) ($n \geq 4$). Significance was tested using a Welch's corrected *t* test (ns: $p > 0.05$, *$0.05 > p > 0.01$, **$0.01 > p > 0.001$, ***$0.001 > p$).

At 37 °C, the amount of internalised peptide corresponds to a fraction internalised by endocytosis and a fraction internalised by direct translocation. At 4 °C, only direct translocation occurs. Assuming that the fraction internalised *via* direct translocation at 37 °C is similar to the amount internalised at 4 °C, it is possible to distinguish between the amount of peptide that entered the cells by endocytosis and by translocation at 37 °C. In wild-type cells, RW9 was mainly internalised *via* endocytosis (80%), whereas in glycosaminoglycan-deficient CHO-pgsA 745 cells, direct translocation accounted for 45% of the total internalised peptide. The situation is even more accentuated for R9, where only translocation (and no endocytosis) occurs in the glycosaminoglycan-deficient cells. Therefore, HS and CS proteoglycans appear to be important for the endocytosis mechanisms of CPPs uptake as was already shown by our laboratory [10]. However, in the absence of these proteoglycans, RW9 is still able to internalise by endocytosis, showing that this peptide uses many distinct pathways (translocation, glycosaminoglycan-dependent and independent endocytosis) to enter cells.

3.3.2. Quantification of membrane-bound peptide

RL9 and RW9 bound to the cell membrane of both cell lines, however RL9 bound to a lesser extent than RW9. For these two peptides, the presence or absence of the proteoglycans at the cell surface seemed to have little effect on their binding to the membrane.

Table 1
Minimum inhibitory concentrations (bacteriostatic) determined for RL9, RW9 and R9 against Gram − *E. coli* and Gram + *S. aureus*.

MIC (μM)	RL9	RW9	R9
E. coli	>100 μM	25 μM	>100 μM
S. aureus	>100 μM	100 μM	>100 μM

At 4 °C, RW9 seemed to bind more to the membrane whereas RL9 seemed to bind less than at 37 °C. The behaviour of R9 was quite different: it bound to the same extent to the cell membrane as RW9 at 37 °C, however, at 4 °C, the amount of bound peptide increased almost three fold.

Overall, the results indicate that the three peptides are able to bind to membranes independently of proteoglycans. At 4 °C, the amount of RW9 and R9 bound to the membrane is higher than at 37 °C. This could be a consequence of the inhibition of cell-membrane trafficking over the 1 h incubation time [10]. Binding to the cell surface would therefore be a purely physical process. R9 would accumulate the most at the cell membrane, followed by RW9 and RL9. Since R9 has more charges than RW9 and RL9, electrostatic interactions between the peptide and the lipids and proteoglycans at the membrane could be involved. But this is not the only factor at stake, since RL9 has the same amount of charges as RW9 and binds considerably less to the membrane. Interestingly, a parallel can be drawn with the peptide affinities for lipid vesicles that were determined using ITC (see Section 3.4).

Regarding the cellular uptake, it was quite unexpected that RW9 and RL9 have very different behaviours. One could think that the tryptophan residues play an important role for internalisation as seen in the case of penetratin, where the replacement of Trp 48 or 56 is deleterious for cellular uptake [2,27] and greatly decreases the peptide's partitioning into octanol [28]. However, tryptophan residues are certainly not essential given that R9 internalises to the same extent as RW9. Nonetheless, the tryptophan residues seem to be important in the case of RW9 as compared to RL9. At this point, we hypothesised that the different uptake behaviour of RW9 and RL9 might be explained from their different structures in contact with lipids and distinct modes of interaction and reorganisation of the lipid bilayer leading us to carry out the biophysical studies described below.

3.4. DSC experiments

3.4.1. Effect of RL9, RW9 and R9 on the thermotropic behaviour of anionic and zwitterionic lipids

Herein, we chose to use the C_{14} acyl chains lipids dimyristoyl phosphatidylcholine (DMPC) and dimyristoyl phosphatidylglycerol (DMPG). Regarding the headgroups, phosphatidylcholine is the major component of eukaryotic cell membranes and therefore constitutes a good model for this system. The external leaflet of eukaryotic cell membranes also possesses anionic lipids such as phosphatidic acid (PA), phosphatidylinositol (PI) and phosphatidylserine (PS) (at very low levels) [29]. Phosphatidylglycerol (PG) was chosen as a representative of anionic lipids in membranes to investigate the role of electrostatic interactions between the peptide and the lipids. Eukaryotic cell membranes are rich in unsaturated fatty acids. However, since the phase transition of these lipids is below 0 °C, it cannot be monitored by DSC (the instrument only works above 0 °C). C_{14} fatty acid chain lipids were chosen because the phase transition of these lipids occurs at room temperature which facilitates handling and study of their phase transition by DSC. Even if this lipid is not a major constituent in cell membranes, it has been widely employed to follow the effects of peptides on lipid phase transitions (see [30] for instance).

Thermograms illustrating the effect of RL9, RW9 and R9 on the thermotropic phase behaviour of DMPC and DMPG MLVs are presented in Fig. 2 and the corresponding thermodynamic parameters are provided in Tables 2–4. Aqueous dispersions of DMPC and DMPG both present two distinct endothermic transitions: a less energetic event around 13 °C corresponding to the transition from the L_{β}' gel phase to the P_{β}' ripple phase and a more energetic event around 24 °C corresponding to the transition between the P_{β}' ripple phase to the L_{α} fluid phase.

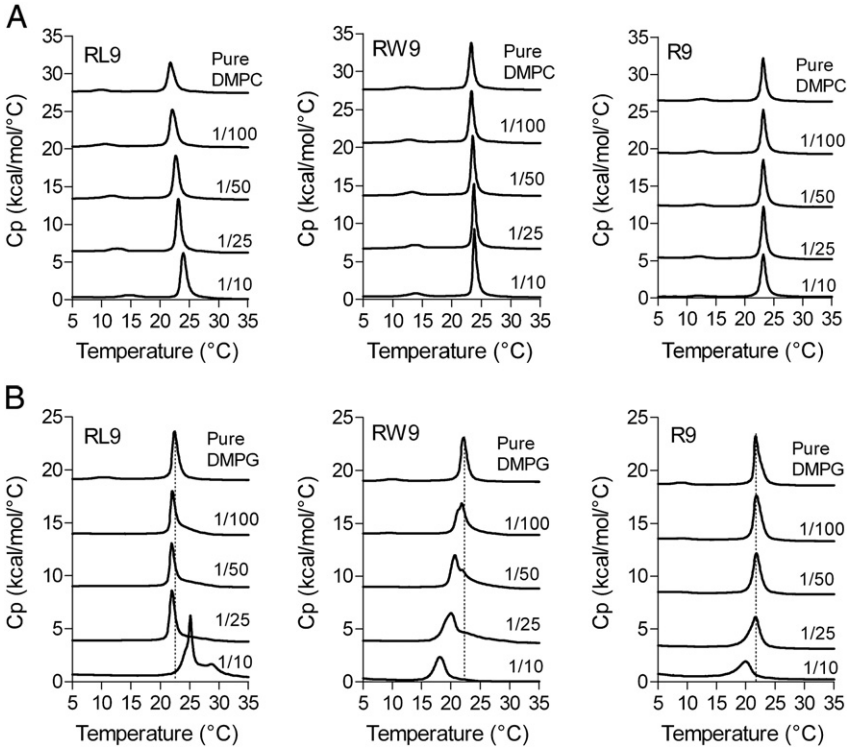

Fig. 2. DSC thermograms illustrating the effect of the addition of RL9, RW9 and R9 to DMPC and DMPG vesicles. (A) Addition of RL9 (left), RW9 (middle) and R9 (right) to DMPC (1 mg/mL). The curves correspond to pure lipid and peptide to lipid ratio of 1:100, 1:50, 1:25 and 1:10. (B) Addition of RL9 (left), RW9 (middle) and R9 (right) to DMPG (1 mg/mL). The curves correspond to pure lipid and peptide to lipid ratio of 1:100, 1:50, 1:25 and 1:10.

Table 2
Thermodynamic parameters obtained by DSC for the interaction of RL9 with MLVs of DMPC, DMPG and DSPG.

Lipid	P/L	T_m (°C)	ΔH_m (kcal/mol)	$\Delta T_{1/2}$ (°C)	T_{pre} (°C)	ΔH_{pre} (kcal/mol)
DMPC	0	23.3	6.7	0.8	12.5	0.8
	1/25	23.7	7.5	0.7	13.8	1.1
DMPG	0	22.4	6.4	0.9	10.4	0.3
	1/25	21.9	7.3	0.9	–	–
DSPG	0	52.4	14.0	0.9	–	–
	1/25	54.0	17.8	1.2	–	–

Table 4
Thermodynamic parameters obtained by DSC for the interaction of R9 with MLVs of DMPC, DMPG and DSPG.

Lipid	P/L	T_m (°C)	ΔH_m (kcal/mol)	$\Delta T_{1/2}$ (°C)	T_{pre} (°C)	ΔH_{pre} (kcal/mol)
DMPC	0	23.2	6.7	0.6	12.6	0.7
	1/25	23.2	8.0	0.7	12.2	0.7
DMPG	0	21.7	6.7	0.8	9.4	0.32
	1/25	21.6	6.9	0.9	–	–
DSPG	0	50.2	13.7	1.0	–	–
	1/25	53.8	18.1	0.9	–	–

All three peptides, R9, RL9 and RW9 only altered the pre-transition or the main transition of DMPC very slightly. In particular, it should be noted that none of the three peptides abolished the pre-transition. This indicates that these peptides do not interact with the polar zwitterionic headgroups of DMPC. The effect of RL9 and RW9 was also tested on another zwitterionic lipid, dimyristoyl phosphatidylethanolamine (DMPE) (data not shown) and no significant interaction could be observed, suggesting that the electrostatic interaction between the lipid and the peptide is crucial. This observation is further discussed in Sections 3.5 and 3.7.

In the case of DMPG, RL9 did not affect the main transition, but the pre-transition disappeared at P/L 1/100. This shows that the peptide only interacts with the lipid headgroups affecting its tilting without affecting the fatty acid chain packing. The interaction of RW9 with DMPG also lead to large changes in the thermotropic behaviour of the lipid with reduction in the phase transition temperature (T_m), the cooperativity and the enthalpy of the pre-transition (which disappears at P/L 1/50). The decrease followed by the disappearance of the pre-transition shows that RW9 interacts with the negatively charged headgroups of DMPG. Decrease in T_m implies that RW9 interacts more favourably with the fluid phase of the lipid rather than with the gel phase. The alteration of the enthalpy of the main transition and the broadening of the peak suggest that the peptide is able to insert into the hydrophobic core of the bilayer and interact with the hydrocarbonated chains of the lipids. A similar trend was observed for R9.

At P/L 1/10 the thermogram often deviated from the trend observed from P/L 1/100 to 1/25,at this very high peptide concentration other phenomena, such as precipitation, may occur and thus these results will not be discussed here.

The eukaryotic cell membrane is composed of regions of different thicknesses. In order to probe the role of the lipid hydrocarbonated chains length in the peptide/lipid interactions, the effect of RL9, RW9 and R9 on the C_{18} acyl chains distearoyl phosphatidylglycerol (DSPG) lipid was tested (Tables 2–4). Due to the pre-transition of DSPG being very close to the main transition [31], it was not possible to study it separately from the main transition. Generally, addition of peptide to DSPG did not have exactly the same effect on the phase transition as for DMPG. For all three peptides, an increase in T_m was observed, together with small variations in enthalpy. Generally, perturbations in the thermogram were weaker for DSPG when compared to DMPG, probably due to the increase in Van der Waals interactions with chain length. The higher perturbation was observed in the case of RW9 probably due to its higher hydrophobicity (Tables 2–4) [28].

Table 3
Thermodynamic parameters obtained by DSC for the interaction of RW9 with MLVs of DMPC, DMPG and DSPG.

Lipid	P/L	T_m (°C)	ΔH_m (kcal/mol)	$\Delta T_{1/2}$ (°C)	T_{pre} (°C)	ΔH_{pre} (kcal/mol)
DMPC	0	23.3	6.3	0.8	10.0	0.6
	1/25	23.1	8.0	0.6	12.6	0.9
DMPG	0	22.2	6.3	1.0	10.0	0.3
	1/25	20.0	8.5	1.6	–	–
DSPG	0	52.3	12.6	0.8	–	–
	1/25	53.3	8.9	0.8	–	–

The thermodynamic parameters obtained from the DSC experiments with RL9, RW9 and RW9 are summarised in Tables 2–4, respectively, for the lipids alone and a peptide to lipid ratio of 1/25.

Overall, the results indicate that an electrostatic recognition between the positively charged arginine residues of the peptides and the anionic lipid headgroups is necessary for their interaction. This correlates well with previous observations by Maiolo and coworkers who reported that the binding of the R7 and R7W peptides to lipid model systems depends strongly on lipid composition and on the presence of negatively charged lipids [32]. When comparing the peptides that are internalised by the cells (R9 and RW9) and the peptide that is not internalised (RL9), the peptides that are internalised promote an increase in the lipid bilayer fluidity (decrease of T_m) whereas the non-internalised peptide does not alter the fluidity of the bilayer (no change of T_m for RL9). Moreover RW9 and R9 perturb considerably more the cooperativity of the lipid phase transition (significant broadening of the transition peak) than RL9 due to a greater disruption of the interactions between the lipid fatty acid chains induced by these peptides. The increase in the fluidity of the lipid bilayer by the R9 and RW9 peptides and subsequent greater perturbation of the cooperativity of the lipid transition may be related with their uptake properties. This will be further discussed below.

3.4.2. Effect of RL9 and RW9 on lipid membrane curvature

Addition of a peptide to a lipid membrane can induce modification in the curvature of the membrane. Changes in curvature are often involved in lipid reorganisation induced by membrane-active peptides and are an important element to consider. Eukaryotic membranes possess up to 10% of phosphatidylethanolamine (PE) in their external leaflet and a small percentage of phosphatidic acid [29]. Both lipids have a small headgroup and have tendency to induce a negative curvature in membranes [33,34]. This can be investigated by observing the shift in transition temperature T_H from the lamellar L_α fluid phase to the hexagonal phase H_{II} of PE lipids. Indeed, a shift of T_H to lower temperature when adding the peptide shows that the apparition of the hexagonal phase is favoured, whereas a shift of T_H to higher temperature indicates that the peptide disfavours a negative curvature.

The effects of RL9, RW9 and R9 on membrane curvature were studied by observing the thermotropic behaviour of dipalmitoleoyl phosphatidylethanolamine (DiPoPE) with or without peptide. DiPoPE is a standard lipid often used because it displays the most energetic L_α to H_{II} transition amongst PE lipids [35]. However, as the lamellar to hexagonal transition of DiPoPE is still quite low in energy, a high concentration of lipid had to be used. The T_H in the absence of peptide was around 42 °C. Addition of RL9 to the lipid had little effect on the T_H. On the other hand, addition of RW9 induced a large shift of T_H to higher temperatures (50 °C) showing that the presence of RW9 strongly disfavours a negative curvature on the lipid membrane. Finally, addition of R9 to DiPoPE slightly decreased the transition temperature to 40.3 °C, R9 would then favour a negative curvature of the bilayer (Fig. 3). These data indicate that RL9 does not affect the

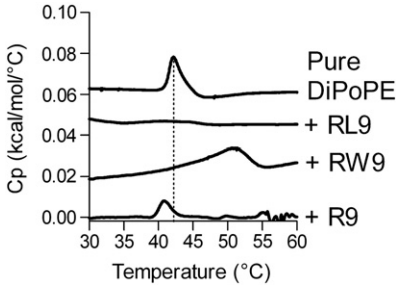

Fig. 3. DSC thermograms illustrating the effect of the addition of RL9, RW9 and R9 to DiPoPE (10 mg/mL). The peptides are added to reach the peptide to lipid ratio of 1:25.

membrane curvature whereas RW9 and R9 do. Variations in enthalpy upon peptide addition due to peptide intercalation between the fatty acid chains were not quantified because of their small magnitude.

3.5. Binding of RL9, RW9 and R9 to large unilamellar vesicles (LUVs)

The interaction of the three studied peptides RL9, RW9 and R9 with phospholipids was also investigated using ITC. The experiments were performed as described by Seelig [36], large unilamellar vesicles of DSPG were injected into the calorimeter cell containing the peptide at 25 °C. From this, the enthalpy of binding of the peptide to the liposome (ΔH) was determined as well as an apparent K_A which represents the affinity of the peptide for the liposome and the stoichiometry of binding n, i.e. the number of phospholipids per peptide. The dissociation constant K_D, the Gibbs free enthalpy (ΔG) and the entropy (ΔS) of binding were derived from the K_A and ΔH. The binding isotherms are presented in Fig. 4, and the resulting thermodynamic parameters are given in Table 5. For the three peptides, binding to DSPG was an exothermic process and therefore, enthalpy driven. RW9 and R9 had a high affinity for the liposome whereas RL9 had a much lower affinity. This correlates well with the membrane-bound peptide quantification reported in Section 3.3, with R9 and RW9 binding more to the cell membrane than RL9. A strong affinity for liposomes of an arginine-rich peptide containing a tryptophan residue, R7W, has also already been reported [32]. Finally, the stoichiometry of binding for R9 was higher, which is consistent with the fact that R9 bears more positive charges than RW9 and RL9. The interaction between RW9, RL9 and R9 with distearoyl phosphatidylcholine (DSPC) liposomes was also investigated, but no binding between the peptides and the liposomes could be observed (results not shown). These results indicate that electrostatic interactions between the positively charged arginines in the peptide and the negatively charged phospholipids headgroups are essential for the peptide/lipid recognition. When considering eukaryotic cell membranes, it should be noted that they do not contain PG, but contain other anionic lipids in the external leaflet of the membrane such as small quantities of PS, PA and PI. Even if they are present at very low levels, these negatively charged lipids contribute to the overall charge of the eukaryotic membrane. They also promote high local concentrations of peptide at the cell surface. Moreover, although we have not investigated this aspect, several studies have shown a high affinity of basic peptides to HS, demonstrating the important role of electrostatic interactions in the peptide/membrane recognition [37,38].

3.6. Changes in LUV turbidity induced by peptide addition

Turbidity experiments (Fig. 5) showed the changes of optical density of suspensions of DMPC or DMPG LUVs with gradual addition of peptide measured at 436 nm. Addition of RL9, RW9 or R9 to DMPC LUVs caused no changes in turbidity, whereas it caused a massive increase in the turbidity of the DMPG LUVs indicating that vesicle aggregation takes place. This experiment was also important to understand possible fluctuation in the structure content of the peptides observed by CD (see below). Indeed, a decrease of secondary structure content was observed when increasing the peptide concentration which can be attributed to a diminution of soluble peptide due to precipitation. We also tried to monitor the size of the aggregates formed after addition of peptide into LUVs suspension by Dynamic Light Scattering (DLS), however, the polydispersity was too high to allow us to draw significant results from these experiments.

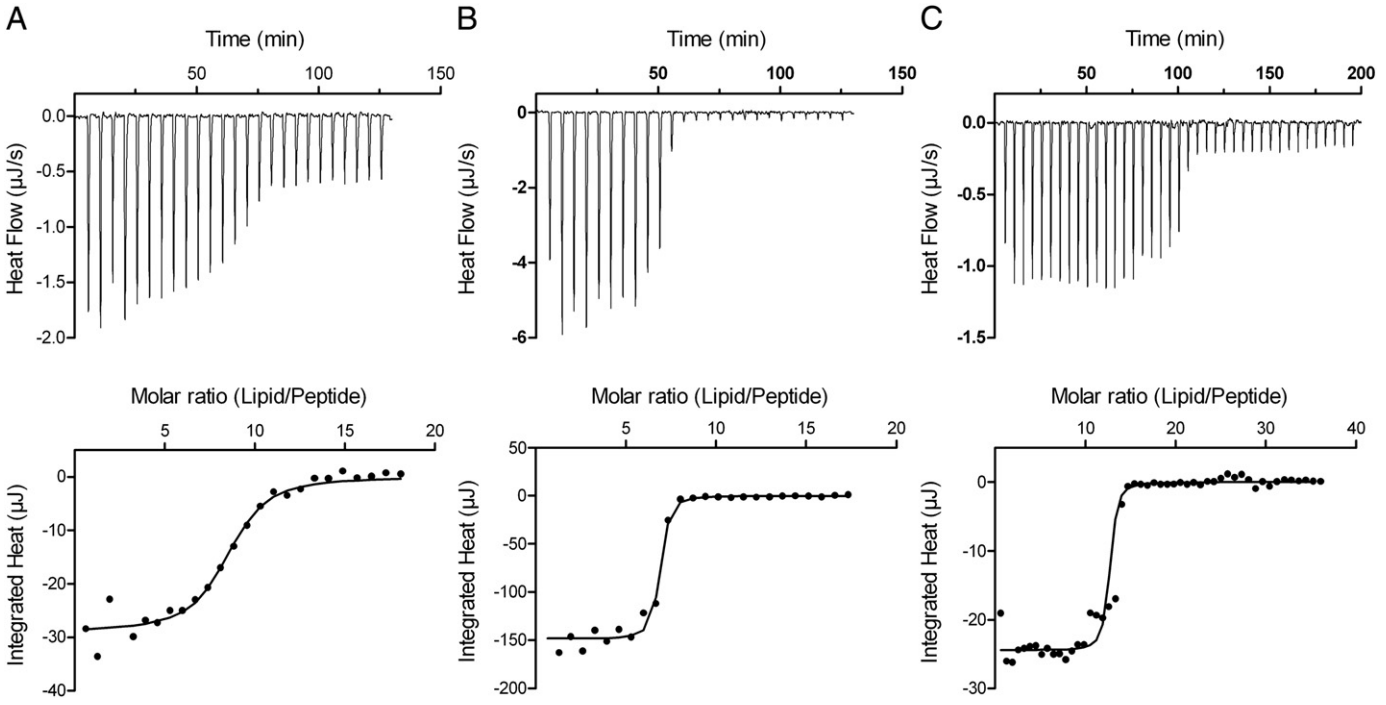

Fig. 4. Isothermal titration of RL9 (A), RW9 (B) and R9 (C) with DSPG LUVs at 25 °C. The lower curves represent the heat of reaction (measured by peak integration) as a function of lipid/peptide molar ratio. The solid lines represent the best fits to experimental data. Thermodynamic parameters calculated from these experiments are presented in Table 5.

Table 5
Thermodynamic parameters of peptides binding to DSPG LUVs determined by ITC at 25 °C.

	RL9	RW9	R9
K_A^{app} (M^{-1})	7.2 10^4	10.5 10^5	8.8 10^5
K_D^{app} (μM)	13.9	0.95	1.14
ΔH (kJ/mol)	−0.46	−2.32	−0.39
ΔG (kJ/mol)	−37.7	−44.3	−43.9
ΔS (kJ/mol/K)	0.12	0.14	0.15
Binding stoichiometry, *n*	8.3	6.4	13.1

3.7. Determination of the secondary structure of the peptides in the presence of lipids by CD

Usually unstructured in aqueous buffer, numerous membrane active peptides tend to adopt a well-defined secondary structure when in contact with lipid membranes. This change in structure can partly explain their membranotropic abilities. In some cases, peptide structuring can even trigger cellular uptake [39]. CD spectroscopy was used to determine the secondary structure of RL9, RW9 and R9 in buffer as well as in presence of zwitterionic and negatively charged bilayers, namely DMPC and DMPG LUVs. Results are displayed in Fig. 6. Qualitative secondary structure assignments were based on the following: α-helix, minima at 208 and 222 nm, maximum at 190 nm; β-sheet, minimum at 218 nm, maximum at 195 nm; random coil, minimum at 198 nm, no positive peak [40].

In buffer conditions, RL9 tended to be mainly unstructured. This was also the case when the peptide was in the presence of DMPC LUVs. However, in the presence of DMPG, the peptide gained an α-helical structure as indicated by the two clear minima at 208 nm and 222 nm on the spectrum. Therefore, RL9 is able to adopt a helical amphipathic structure only in the presence of negative charges. RW9 had partial helical content in buffer, and its secondary structure was not sensibly modified in the presence of DMPC. Indeed, a slight minimum at 222 nm can be observed on the corresponding spectra. However, in the presence of DMPG, the CD signature changed significantly, with two deep minima appearing at 205 nm and 228 nm and a maximum at 215 nm. This unusual spectrum likely arises from the presence of the tryptophan residues interacting with the peptide backbone or stacking [41], but no definite structure can be attributed. Such signals were reported in the literature for the tryptophan-rich antimicrobial peptides indolicidin and tritrypticin and were interpreted as beta turn structures [42–44]. However these tryptophan-rich peptides contain proline residues which are consistent with such a structure as opposed to RW9 which only contains arginine and tryptophan residues. Therefore, the structure of RW9 in the presence of DMPG could not be easily determined using CD spectroscopy and was further investigated using NMR. Since NMR experiments cannot be performed with liposomes which are too large objects, we employed dodecyl phosphocholine (DPC), dioctanoyl phosphatidylglycerol (D8PG) and sodium dodecyl sulfate (SDS) as model systems (the reason for the choice of those molecules is provided below).

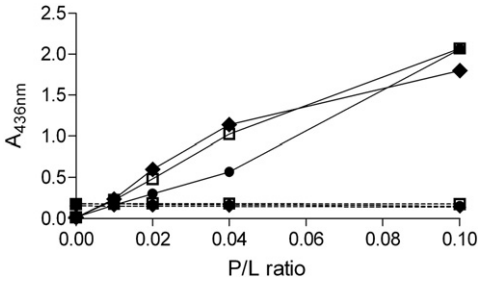

Fig. 5. Turbidity changes induced by addition of RL9 (squares), RW9 (dots) and R9 (diamonds) to DMPC (hatched line) and DMPG (solid line) LUVs.

Therefore, CD spectra of RW9 and RL9 in the presence of such model systems were also recorded (Fig. 7). In the presence of SDS RW9 was structured in α-helix, whereas in the case of DPC there was a mixture of helical structures with the signal typical of tryptophan-rich peptides. The tryptophan contribution to the CD signal became more intense in the case of D8PG, similarly to what was observed with DMPG.

R9 was mostly unstructured in solution and in the presence of DMPC but became partly structured in the presence of DMPG with a CD signal close to an α-helix signal. However the signal is not the signature of a pure helix since the minima are not at 208 and 222 nm but are slightly shifted towards 205 and 220 nm, indicating the presence of other states such as random coil conformation [45]. These small displacements of the absorbance minima were also observed in the case of RW9 in buffer and with DMPC.

These observations show that in our studies structuring of the peptide in the presence of lipids is not directly linked to its biological properties. It is interesting to see that RL9 gains an amphipathic helical structure in the presence of negatively charged lipids but is neither a CPP nor an antimicrobial peptide. As regards to RW9, the situation is more complicated as the CD data could not provide us with a definite structure for this peptide.

3.8. Peptides secondary structure determination in presence of membrane-mimetic systems by NMR

Since the CD spectra of RW9 exhibited atypical signatures, the conformations of RW9 and RL9 peptides were further investigated by NMR spectroscopy in aqueous and in micellar solutions. Proton sequence-specific resonance assignments were obtained using standard procedures based on the analysis of homonuclear 2D TOCSY (through bond) and 2D NOESY (through space) correlation experiments. Natural abundance 2D ^{1}H-^{13}C HSQC spectra was also recorded to facilitate side-chain assignments and provide additional conformational parameters. Preliminary information on the peptide structure was first inferred from the analysis of the chemical shift deviations (CSDs) of $^1H^{\alpha}$ and $^{13}C^{\alpha}$ resonances. Indeed, these CSDs, defined as the differences between observed chemical shifts of each amino acid and corresponding random coil values [46], are good indicators of the local conformational propensities of each residue [47].

The RW9 and RL9 peptides show little ^{1}H, ^{13}C chemical shift dispersion and small CSDs of C^{α} resonances in aqueous solutions (Fig. 8), indicative of random coil conformations. The upfield shifts of H^{α} resonances (average value of −0.2 ppm) observed in RW9 are probably due to aromatic ring current effects of the three Trp residues, since the CSDs of corresponding C^{α} resonances show near zero values. Therefore the secondary structure analysis was mainly based on C^{α} CSDs for this peptide. The absence of preferential conformations is further confirmed by the averaged values of $^3J_{HN\text{-}H\alpha}$ coupling constants (~7 Hz), together with the pattern of intraresidual and sequential backbone NOEs: sequential $H\alpha_i$–HN_{i+1} NOEs stronger than intraresidual $H\alpha_i$–HN_i NOEs, weak sequential HN_i–HN_{i+1} NOEs. These results are in good agreement with the CD data.

3.8.1. RW9 peptide in micellar environments

The addition of DPC or SDS micelles causes a large chemical shift dispersion of amide and aromatic resonances and a broadening of resonances (Fig. S2), indicating that the RW9 peptide interacts with the detergent micelles and undergoes significant conformational changes. The addition of D8PG micelles caused a precipitation of peptide–detergent complexes, preventing the NMR study. The chemical shift dispersion of ^{1}H resonances is larger in DPC micelles than in SDS micelles and the chemical shift changes of the indole $HN^{\varepsilon 1}$ protons differ in the two detergents, reflecting variations of environments for the Trp residues. Continuous stretches of upfield shifts of H^{α} resonances and

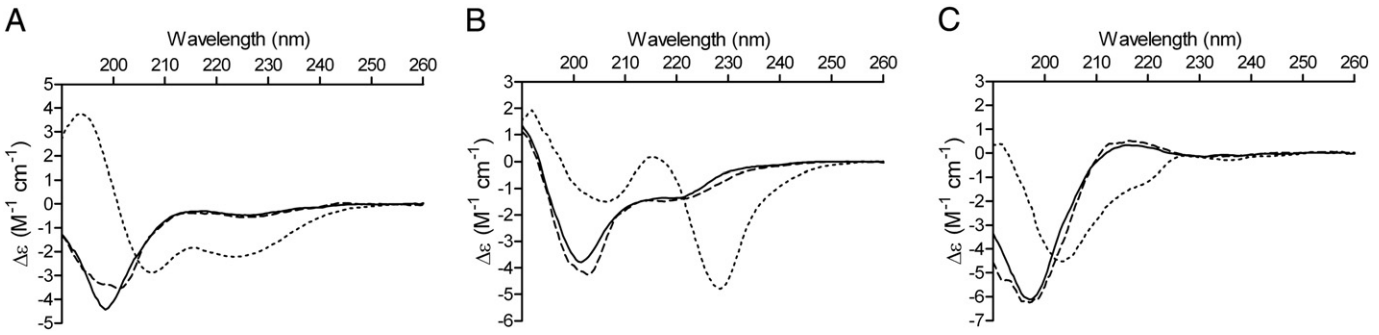

Fig. 6. CD spectra of RL9 (A), RW9 (B) and R9 (C) in 10 mM sodium phosphate buffer (solid line), DMPC LUVs (hatched line) and DMPG (dotted line) at P/L ratio of 1/25 measured at 20 °C.

downfield shifts of C^{α} resonances are observed throughout the sequence, showing that the RW9 peptide adopts helical conformations in the presence of detergents (Fig. 8). Assuming an average C^{α} CSD value of 2.6 ppm in helices [47], the amount of helicity was estimated to 67% in DPC and 27% in SDS micelles. The smaller helix content observed in SDS is in agreement with the CD data. The C^{α} CSDs are smaller for the last two residues of RW9 in DPC, indicating a loosening of the helix in the C-terminal part. The helix adopted by RW9 in the anionic SDS detergent is less stable, residues in the N-terminal half showing the highest helical propensity. The helical conformation of RW9 peptide is further supported by the pattern of intraresidual and sequential NOEs observed in both detergent systems, namely strong HN_i–HN_{i+1} and $H\alpha_i$–HN_i NOEs, and medium $H\alpha_i$–HN_{i+1} NOEs, together with characteristic medium-range $H\alpha_i$–HN_{i+3} and $H\alpha_i$–HN_{i+4} NOEs (Fig. 9).

Differences in the conformations of RW9 side-chains are also observed in the two detergent systems, as revealed by NOEs involving side-chain protons. In DPC micelles, numerous NOEs involving Trp aromatic protons are observed, in particular with Arg side-chain methylenic protons. This indicates the presence of persistent cation-π interactions between Arg and Trp side-chains. In contrast, in SDS micelles, the NOEs involving Trp aromatic protons are less numerous and of weaker intensity.

The NMR structures of RW9 in both solvents were calculated by restrained molecular dynamics in DYANA and refined by energy minimisation with XPLOR-NIH and CHARMM22 forcefield (Fig. 10). The rmsd calculated on backbone atom positions is 0.35 and 0.84 Å, for the structures in DPC and SDS respectively. The peptides adopt well-defined amphipathic helices, with a large polar sector. The side-chain conformations are better defined in the family structure in DPC. Cation-π interactions are observed in different conformers of the NMR structure family in DPC. Especially, Arg8 residue was found to interact preferentially with Trp4 and Trp7. This is in agreement with the upfield shifted resonances of its H^{γ} and H^{δ} protons, in comparison with other Arg residues. The interactions observed between side-chains slightly differ for the NMR structure ensemble in SDS. This result is confirmed by the analysis of Arg side chain chemical shifts, residue Arg5 exhibiting the most upfield shifted resonances. These differences in side-chain interactions observed in zwitterionic and anionic micelles, as revealed by NMR spectroscopy, enable us to re-examine the CD data. Indeed, the large discrepancy in the CD spectra in DPC and SDS micelles can be ascribed to different helical contents, together with different orientations of Trp chromophores that can be involved in π-π or π-cation interactions. The negative band at 228 nm in the CD spectra is consistent with interactions between Trp side chains [41,42]. This contribution is smaller in anionic SDS micelles, which can be explained by less well defined side chain orientations.

3.8.2. RL9 peptide in micellar environments

The RL9 peptide also adopts helical conformations in the presence of DPC or SDS micelles, as shown by the CSDs (Fig. 8) and pattern of NOEs (Fig. 9). The amount of helicity, as inferred by C^{α} CSDs, is 75% in DPC and 53% in SDS. The CSDs of H^{α} protons yield close values of 75% and 38% of helix in DPC and SDS, respectively, based on an average H^{α} CSD value of 0.35 ppm in helices [47]. The helical propensity decreases in the C-terminal part in both detergent systems. The NMR structure of RL9 in DPC (Fig. 10) shows a well-defined amphipathic helix for residues 1–7, with a small hydrophobic sector and a larger polar face. The characterisation of medium-range Hα–HN NOEs in SDS was hampered by the very small chemical shift dispersion of H^{α} resonances. Therefore structures were not calculated in SDS, due to the short number of assigned medium-range NOEs.

4. Conclusions

Herein, we have studied the cell membrane binding and cell uptake of three arginine-rich peptides: the classic R9 and two amphipathic peptides with the same charge distribution composed of six arginines and three leucines or three tryptophans, RL9 or RW9, respectively. To distinguish between the peptide internalised by direct translocation and by endocytosis, quantification of peptide uptake by

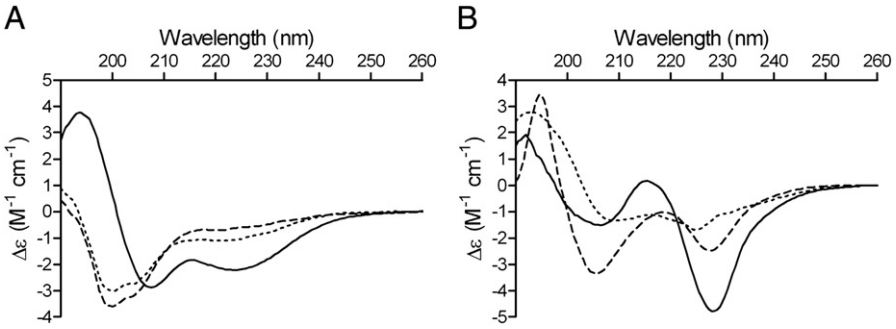

Fig. 7. CD spectra of RL9 (A) and RW9 (B) in the presence of DMPG (solid line), DPC (hatched line) and SDS (dotted line) at a peptide concentration of 50 μM, measured at 20 °C.

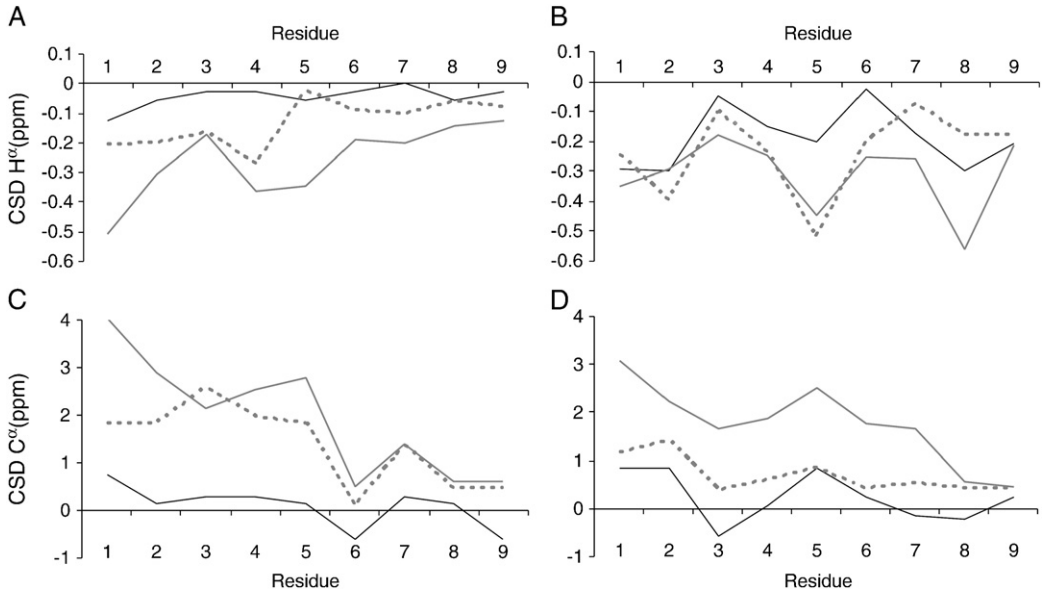

Fig. 8. $^{1}H^{\alpha}$ and $^{13}C^{\alpha}$ Chemical Shift Deviations (CSDs) of RL9 (A, C) and RW9 (B, D) peptides in sodium phosphate buffer (solid lines), in DPC micelles (solid grey lines) and in SDS micelles (hatched grey lines).

CHO cells was performed at 4 °C (translocation only) and 37 °C (translocation and endocytosis). Furthermore, to investigate the role of HS and CS proteoglycans, the experiments were performed in cells expressing (CHO-K1) or not (CHO-pgsA745) glycosaminoglycans at their surface. We have shown that while R9 and RW9 internalise in both cell lines, at 4 °C and 37 °C, RL9 does not, even if it binds slightly to the cell membrane. The fact that RL9 does not internalise in cells is very surprising since previous studies with a quite similar peptide (RLRRLRRLRR) have shown that it is able to enter cells [48]. This peptide possesses one more arginine residue than RL9, but this should not be sufficient to explain differences in uptake between these two sequences, since studies have shown that a minimum of six charges is sufficient for CPP internalisation [49,50]. These contradictory results could be explained by the fact that quantification of the cellular uptake of the RLRRLRRLRR sequence was performed using Fluorescence-activated cell sorting (FACS), which cannot distinguish between the peptide that is bound to the membrane and peptide that is internalised by cells, unlike the protocol using mass spectrometry quantification we applied in our study. Arginine-rich peptides being highly positively charged, they can bind strongly to membranes, moreover, the guanidinium group has special affinity for the polar headgroups of phospholipids [28,51], and indeed, we have observed that RL9 binds to the cell membrane. Washing the cells after incubation with peptide may not be sufficient to remove all membrane-bound peptides, and proteolytic digestion of these extracellular peptides avoids subsequent overestimation of the amount of internalised peptide. This is a valuable example to show that extreme caution must be taken when analysing CPP cellular uptake by fluorescence methods with no external peptide digestion or no fluorescence quenching by Trypan blue [52] since the presence of fluorescence likely arises from peptides that are just bound to the membrane but not internalised [10].

In attempt to rationalise the different internalisation behaviour of RL9 as compared to RW9 and R9, we investigated the interaction of these peptides and their effects on the organisation of lipid membranes using lipid model systems. Both R9 and RW9 are able to cross the cell membrane *via* direct translocation, even though it is not the major pathway for RW9. In any case, translocation or endocytosis, the cell membrane is the first obstacle that the peptide will encounter. Overall our results demonstrate that the electrostatic interaction between the peptides and lipids plays a major role as they lead to a decrease in the Born energy barrier [28,51]. Independently from their structure, the internalised peptides (R9 and RW9) have more affinity for negatively charged membranes than the peptide that is not internalised (RL9). RW9 and R9 also increase the bilayer fluidity and affect the fatty acid chain packing more than RL9. An increase in the lipid bilayer fluidity renders the bilayer more prone to lipid supramolecular reorganisation (e.g. formation of lipid domains, membrane bending and curvature) and protein rearrangements occurring during peptide translocation and

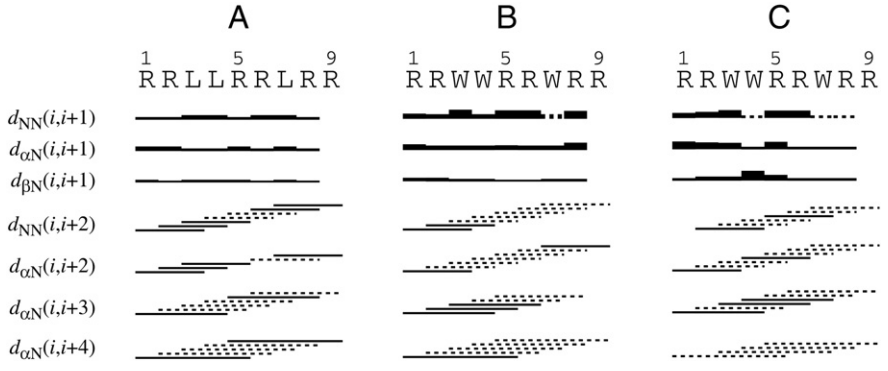

Fig. 9. Diagram of backbone NOEs observed for RL9 in DPC micelles (A), and RW9 in DPC (B) or in SDS (C) micelles. The relative intensity of NOE connectivities is indicated by horizontal bars of varying thickness. Solid lines correspond to unambiguously assigned NOEs and dotted lines represent ambiguous NOEs due to spectral overlap.

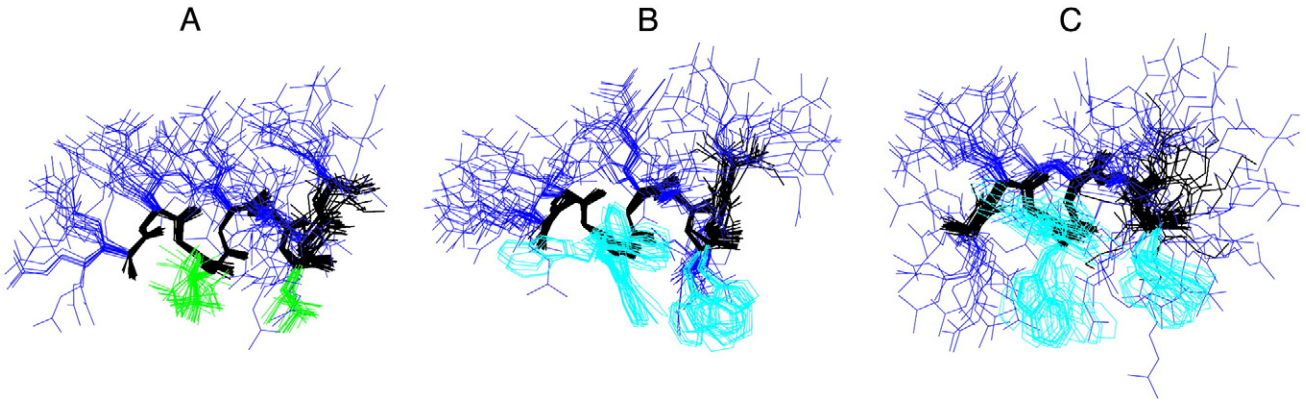

Fig. 10. 3D NMR structures of RL9 in DPC micelles (A), and RW9 in DPC (B) or SDS (C) micelles. Structures were superimposed by best fitting of backbone atoms of residues 1–7. Backbone atoms are shown in black. Side-chain atoms are shown in dark blue (Arg residues), green (Leu residues) or light blue (Trp residues).

endocytosis. This could partially explain the differences in uptake observed between R9 and RW9 and RL9.

Supplementary materials related to this article can be found online at doi:10.1016/j.bbamem.2010.09.009.

Acknowledgments

This work was supported by the Association Nationale pour la Recherche (ANR-Prob DOM) and the Ministère de l'Enseignement Supérieur et de la Recherche. We thank Dr. Véronique Peyre for her help with DLS. Also we want to thank Dr. Sylvie Rebuffat (Muséum d'Histoire Naturelle) for providing us with the *E. coli* ML35p strain and Dr. Tarek Masdek and Mélanie Falord (Institut Pasteur) for giving us the *S. aureus* RN4220 strain.

References

[1] S.B. Fonseca, M.P. Pereira, S.O. Kelley, Recent advances in the use of cell-penetrating peptides for medical and biological applications, Adv. Drug Deliv. Rev. 61 (2009) 953–964.
[2] D. Derossi, A.H. Joliot, G. Chassaing, A. Prochiantz, The third helix of the Antennapedia homeodomain translocates through biological membranes, J. Biol. Chem. 269 (1994) 10444–10450.
[3] D. Derossi, S. Calvet, A. Trembleau, A. Brunissen, G. Chassaing, A. Prochiantz, Cell internalization of the third helix of the Antennapedia homeodomain is receptor-independent, J. Biol. Chem. 271 (1996) 18188–18193.
[4] S. Fawell, J. Seery, Y. Daikh, C. Moore, L.L. Chen, B. Pepinsky, J. Barsoum, Tat-mediated delivery of heterologous proteins into cells, Proc. Natl Acad. Sci. USA 91 (1994) 664–668.
[5] A.D. Frankel, C.O. Pabo, Cellular uptake of the tat protein from human immunodeficiency virus, Cell 55 (1988) 1189–1193.
[6] D.J. Mitchell, D.T. Kim, L. Steinman, C.G. Fathman, J.B. Rothbard, Polyarginine enters cells more efficiently than other polycationic homopolymers, J. Pept. Res. 56 (2000) 318–325.
[7] P.A. Wender, D.J. Mitchell, K. Pattabiraman, E.T. Pelkey, L. Steinman, J.B. Rothbard, The design, synthesis, and evaluation of molecules that enable or enhance cellular uptake: peptoid molecular transporters, Proc. Natl Acad. Sci. USA 97 (2000) 13003–13008.
[8] D. Derossi, G. Chassaing, A. Prochiantz, Trojan peptides: the penetratin system for intracellular delivery, Trends Cell Biol. 8 (1998) 84–87.
[9] D. Delaroche, B. Aussedat, S. Aubry, G. Chassaing, F. Burlina, G. Clodic, G. Bolbach, S. Lavielle, S. Sagan, Tracking a new cell-penetrating (W/R) nonapeptide, through an enzyme-stable mass spectrometry reporter tag, Anal. Chem. 79 (2007) 1932–1938.
[10] C.Y. Jiao, D. Delaroche, F. Burlina, I.D. Alves, G. Chassaing, S. Sagan, Translocation and endocytosis for cell-penetrating peptide internalization, J. Biol. Chem. 284 (2009) 33957–33965.
[11] F. Burlina, S. Sagan, G. Bolbach, G. Chassaing, Quantification of the cellular uptake of cell-penetrating peptides by MALDI-TOF mass spectrometry, Angew. Chem. Int. Ed Engl. 44 (2005) 4244–4247.
[12] S.T. Henriques, M.N. Melo, M.A. Castanho, Cell-penetrating peptides and antimicrobial peptides: how different are they? Biochem. J. 399 (2006) 1–7.
[13] F. Burlina, S. Sagan, G. Bolbach, G. Chassaing, A direct approach to quantification of the cellular uptake of cell-penetrating peptides using MALDI-TOF mass spectrometry, Nat. Protoc. 1 (2006) 200–205.
[14] S.P. Rucker, A.J. Shaka, Broadband homonuclear cross polarization in 2D NMR using DIPSI-2, Mol. Phys. 58 (1989).
[15] V. Sklenar, M. Piotto, R. Leppik, V. Saudek, Gradient-tailored water suppression for 1H-15N HSQC experiments optimized to retain full sensitivity, J. Magn. Reson. A 102 (1993).
[16] G. Lippens, C. Dhalluin, J.M. Wieruszeski, Use of a water flip-back pulse in the homonuclear NOESY experiment, J. Biomol. NMR 5 (1995).
[17] T.L. Hwang, A.J. Shaka, Water suppression that works. Excitation sculpting using arbitrary waveforms and pulsed field gradients, J. Magn. Reson. A 112 (1995) 275–279.
[18] P. Guntert, C. Mumenthaler, K. Wuthrich, Torsion angle dynamics for NMR structure calculation with the new program DYANA, J. Mol. Biol. 273 (1997) 283–298.
[19] C.D. Schwieters, J.J. Kuszewski, N. Tjandra, G.M. Clore, The Xplor-NIH NMR molecular structure determination package, J. Magn. Reson. 160 (2003) 65–73.
[20] C. Palm, S. Netzereab, M. Hallbrink, Quantitatively determined uptake of cell-penetrating peptides in non-mammalian cells with an evaluation of degradation and antimicrobial effects, Peptides 27 (2006) 1710–1716.
[21] B. Bechinger, K. Lohner, Detergent-like actions of linear amphipathic cationic antimicrobial peptides, Biochim. Biophys. Acta 1758 (2006) 1529–1539.
[22] I. Zelezetsky, S. Pacor, U. Pag, N. Papo, Y. Shai, H.G. Sahl, A. Tossi, Controlled alteration of the shape and conformational stability of alpha-helical cell-lytic peptides: effect on mode of action and cell specificity, Biochem. J. 390 (2005) 177–188.
[23] P.E. Thoren, D. Persson, P. Isakson, M. Goksor, A. Onfelt, B. Norden, Uptake of analogs of penetratin, Tat(48-60) and oligoarginine in live cells, Biochem. Biophys. Res. Commun. 307 (2003) 100–107.
[24] I. Nakase, M. Niwa, T. Takeuchi, K. Sonomura, N. Kawabata, Y. Koike, M. Takehashi, S. Tanaka, K. Ueda, J.C. Simpson, A.T. Jones, Y. Sugiura, S. Futaki, Cellular uptake of arginine-rich peptides: roles for macropinocytosis and actin rearrangement, Mol. Ther. 10 (2004) 1011–1022.
[25] T. Suzuki, S. Futaki, M. Niwa, S. Tanaka, K. Ueda, Y. Sugiura, Possible existence of common internalization mechanisms among arginine-rich peptides, J. Biol. Chem. 277 (2002) 2437–2443.
[26] H.L. Lee, E.A. Dubikovskaya, H. Hwang, A.N. Semyonov, H. Wang, L.R. Jones, R.J. Twieg, W.E. Moerner, P.A. Wender, Single-molecule motions of oligoarginine transporter conjugates on the plasma membrane of Chinese hamster ovary cells, J. Am. Chem. Soc. 130 (2008) 9364–9370.
[27] P.M. Fischer, N.Z. Zhelev, S. Wang, J.E. Melville, R. Fahraeus, D.P. Lane, Structure-activity relationship of truncated and substituted analogues of the intracellular delivery vector Penetratin, J. Pept. Res. 55 (2000) 163–172.
[28] E.K. Esbjorner, P. Lincoln, B. Norden, Counterion-mediated membrane penetration: cationic cell-penetrating peptides overcome Born energy barrier by ion-pairing with phospholipids, Biochim. Biophys. Acta 1768 (2007) 1550–1558.
[29] A. Zachowski, Phospholipids in animal eukaryotic membranes: transverse asymmetry and movement, Biochem. J. 294 (Pt 1) (1993) 1–14.
[30] R.N. McElhaney, Differential scanning calorimetric studies of lipid–protein interactions in model membrane systems, Biochim. Biophys. Acta 864 (1986) 361–421.
[31] Y.P. Zhang, R.N. Lewis, R.N. McElhaney, Calorimetric and spectroscopic studies of the thermotropic phase behavior of the n-saturated 1, 2-diacylphosphatidylglycerols, Biophys. J. 72 (1997) 779–793.
[32] J.R. Maiolo, M. Ferrer, E.A. Ottinger, Effects of cargo molecules on the cellular uptake of arginine-rich cell-penetrating peptides, Biochim. Biophys. Acta 1712 (2005) 161–172.
[33] E.E. Kooijman, V. Chupin, B. de Kruijff, K.N. Burger, Modulation of membrane curvature by phosphatidic acid and lysophosphatidic acid, Traffic 4 (2003) 162–174.
[34] M.W. Tate, E.F. Eikenberry, D.C. Turner, E. Shyamsunder, S.M. Gruner, Nonbilayer phases of membrane lipids, Chem. Phys. Lipids 57 (1991) 147–164.
[35] R.M. Epand, R.F. Epand, Modulation of membrane curvature by peptides, Biopolymers 55 (2000) 358–363.
[36] J. Seelig, Titration calorimetry of lipid–peptide interactions, Biochim. Biophys. Acta 1331 (1997) 103–116.

[37] E. Goncalves, E. Kitas, J. Seelig, Binding of oligoarginine to membrane lipids and heparan sulfate: structural and thermodynamic characterization of a cell-penetrating peptide, Biochemistry 44 (2005) 2692–2702.
[38] S.M. Fuchs, R.T. Raines, Pathway for polyarginine entry into mammalian cells, Biochemistry 43 (2004) 2438–2444.
[39] F. Duchardt, I.R. Ruttekolk, W.P. Verdurmen, H. Lortat-Jacob, J. Burck, H. Hufnagel, R. Fischer, M. van den Heuvel, D.W. Lowik, G.W. Vuister, A. Ulrich, M. de Waard, R. Brock, A cell-penetrating peptide derived from human lactoferrin with conformation-dependent uptake efficiency, J. Biol. Chem. 284 (2009) 36099–36108.
[40] S.M. Kelly, T.J. Jess, N.C. Price, How to study proteins by circular dichroism, Biochim. Biophys. Acta 1751 (2005) 119–139.
[41] R.W. Woody, Contributions of tryptophan side chains to the far-ultraviolet circular dichroism of proteins, Eur. Biophys. J. 23 (1994) 253–262.
[42] V.V. Andrushchenko, H.J. Vogel, E.J. Prenner, Solvent-dependent structure of two tryptophan-rich antimicrobial peptides and their analogs studied by FTIR and CD spectroscopy, Biochim. Biophys. Acta 1758 (2006) 1596–1608.
[43] A.S. Ladokhin, M.E. Selsted, S.H. White, CD spectra of indolicidin antimicrobial peptides suggest turns, not polyproline helix, Biochemistry 38 (1999) 12313–12319.
[44] S. Nagpal, V. Gupta, K.J. Kaur, D.M. Salunke, Structure-function analysis of tritrypticin, an antibacterial peptide of innate immune origin, J. Biol. Chem. 274 (1999) 23296–23304.
[45] S.Y. Venyaminov, Determination of Protein Secondary Structure, in: G.D. Fasman (Ed.), Circular Dichroism and the Conformational Analysis of Biomolecules, Plenum Press, New York, 1996.
[46] D.S. Wishart, C.G. Bigam, A. Holm, R.S. Hodges, B.D. Sykes, 1H, 13C and 15N random coil NMR chemical shifts of the common amino acids. I. Investigations of nearest-neighbor effects, J. Biomol. NMR 5 (1995) 67–81.
[47] D.S. Wishart, B.D. Sykes, Chemical shifts as a tool for structure determination, Meth. Enzymol. 239 (1994) 363–392.
[48] J.B. Rothbard, E. Kreider, C.L. VanDeusen, L. Wright, B.L. Wylie, P.A. Wender, Arginine-rich molecular transporters for drug delivery: role of backbone spacing in cellular uptake, J. Med. Chem. 45 (2002) 3612–3618.
[49] S. Futaki, Arginine-rich peptides: potential for intracellular delivery of macromolecules and the mystery of the translocation mechanisms, Int. J. Pharm. 245 (2002) 1–7.
[50] J.B. Rothbard, T.C. Jessop, R.S. Lewis, B.A. Murray, P.A. Wender, Role of membrane potential and hydrogen bonding in the mechanism of translocation of guanidinium-rich peptides into cells, J. Am. Chem. Soc. 126 (2004) 9506–9507.
[51] H.L. Amand, K. Fant, B. Norden, E.K. Esbjorner, Stimulated endocytosis in penetratin uptake: effect of arginine and lysine, Biochem. Biophys. Res. Commun. 371 (2008) 621–625.
[52] N.P. Innes, G.R. Ogden, A technique for the study of endocytosis in human oral epithelial cells, Arch. Oral Biol. 44 (1999) 519–523.